DENOISING AND SPIKE REMOVAL FROM RAMAN SPECTRA USING DOUBLE DENSITY DUAL-TREE COMPLEX WAVELET TRANSFORM

T. S. Sharan, Sh. Sharma*, N. Sharma

School of Biomedical Engineering at Indian Institute of Technology (BHU),
Varanasi-221003, Uttar Pradesh, India; e-mail: tareshss.rs.bme16@itbhu.ac.in,
shiru.bme@itbhu.ac.in, neeraj.bme@itbhu.ac.in

    We aim to show the effectiveness of the double density dual-tree complex wavelet transform to denoise the Raman signal. A comparative study is carried out of the double density dual-tree complex wavelet transform with the discrete wavelet transform, dual tree complex wavelet transforms, and Savitzky–Golay smoothing method to show its capability and effectiveness. Results show that denoising based on the double density dual-tree complex wavelet transform can improve the quantitative and qualitative analysis of the Raman signal.

    Keywords: *Raman spectroscopy, spike removal, denoising, double density dual-tree complex wavelet transform, Savitzky–Golay smoothing.*

УДАЛЕНИЕ ШУМОВ И ВЫБРОСОВ ИЗ СПЕКТРОВ КОМБИНАЦИОННОГО РАССЕЯНИЯ С ИСПОЛЬЗОВАНИЕМ ДВОЙНОГО КОМПЛЕКСНОГО ВЕЙВЛЕТ-ПРЕОБРАЗОВАНИЯ ДВОЙНОЙ ПЛОТНОСТИ

T. S. Sharan, Sh. Sharma*, N. Sharma

УДК 535.375.5

Школа биомедицинской инженерии Индийского технологического института (BHU),
Варанаси-221003, Уттар-Прадеш, Индия; e-mail: tareshss.rs.bme16@itbhu.ac.in,
shiru.bme@itbhu.ac.in, neeraj.bme@itbhu.ac.in

    Предложен метод двойного комплексного вейвлет-преобразование двойной плотности для по-давления шума в сигнале КР. Проведено сравнительное исследование двойного комплексного вейвлет-преобразования двойной плотности с дискретным вейвлет-преобразованием, двойным комплексным вейвлет-преобразованием и методом сглаживания по Савицкому–Голею. Шумоподавление на основе двойного комплексного вейвлет-преобразования двойной плотности может улучшить количествен-ный и качественный анализ сигнала КР.

    Ключевые слова: *спектроскопия комбинационного рассеяния, удаление выбросов, шумоподавле-ние, двойное комплексное вейвлет-преобразование двойной плотности, сглаживание по Савицкому–Голею.*

    Introduction. When monochromatic light interacts with a molecule, the scattered radiation consists of almost the same energy (frequency) component, called Rayleigh scattering. Apart from that, there is radia-tion above and below this fundamental frequency; this phenomenon is known as Raman scattering [1, 2]. Its application for the measurement of chemical and physical properties of material has increased rapidly during the last two decades [3–5]. It is a powerful, non-destructive, and marker-free optical method that relays mo-lecular vibration information of the sample. Different groups have different vibrational energies, and so a unique Raman spectrum is obtained for every molecule. Molecular-level investigation of the sample is pos-sible for Raman spectroscopy and thus provides a 'fingerprint' spectral pattern specific to the molecule of in-terest [6–10]. The spectral analysis becomes difficult if the noise of the non-stationary characteristic is pre-sent. Carrying out an experiment in optimal conditions and averaging over a long time is recommended to reduce noise from the spectrum. But it is not always possible to have these conditions due to different con-straints leading to the introduction of noise in the spectrum.

Charge-coupled devices (CCD) are used in most dispersive Raman spectrometers because of benefits like high quantum efficiency, good sensitivity, high dynamic range and reliability, and small thermal noise [7, 8]. But CCD detectors are sensitive to cosmic rays, leading to large sharp spikes in the spectra [9, 10]. Spikes are randomly distributed in time and space, making it difficult to remove them. The presence of such spurious spikes may introduce a deleterious effect in further analysis of the signal. Thus, it is required to automatically identify and remove spikes from the spectra.

Techniques so far reported in the literature for removal of spikes can be categorized as (i) additional acquisition-based method, (ii) hardware-based methods, and (iii) software-based methods. In the additional acquisition-based method, it is assumed that the probability of occurrence of a cosmic spike at the same pixel in successive measurement is low. The hardware-based method includes methods such as analyzing the full CCD image, image curvature correction, and division of spectrograph slit. But this technique makes the system complex and costly [11]. Thus, software-based spike removal techniques are generally used for Raman spectra.

Signals are inherently corrupted by noise but are neglected because of the high signal to noise ratio (SNR). In Raman spectroscopy, neglecting the noise will influence further analysis and may introduce incorrect information and classification of the sample [12–14]. Raman spectra can be corrupted by various types of noises like dark current noise, analog to digital converter (ADC) noise, fluorescence background, and random noises. Among these, noise due to fluorescence background and random noise are dominant. Only Random noise is considered here.

Let us consider a noisy Raman signal x, which can be represented as

$$x = s + (n_g + n_s),\tag{1}$$

where s denotes the actual Raman signal, n_g denotes the additive white Gaussian noise, and n_s is a spike superimposed on the actual Raman signal. Noise is called additive because it is added to any noise that might be intrinsic to a system, and white refers to the uniform power across the frequency band. Noise can take a value that is Gaussian distributed, the so-called Gaussian noise. The probability density function P of the Gaussian random variable z is given by

$$P(z) = \frac{1}{\sigma\sqrt{2\pi}} e^{-\frac{(z-\mu)^2}{2\sigma^2}},\tag{2}$$

where μ is mean deviation and σ is the standard deviation, here, the denoising operation is applied to obtain the actual Raman signal s from the noisy signal x. Raman signal pre-processing consists of three main steps:

Noisy Signal I/P $\rightarrow$ Normalization $\rightarrow$ Background correction $\rightarrow$ Noise removal $\rightarrow$ Denoised Signal.

Denoising has been a major challenge in the signal pre-processing. Several denoising methods have already been proposed, among which the polynomial least-squares smoothing filter, also known as Savitzky–Golay smoothing, is most commonly used for the Raman signal [15]. It dynamically fits a polynomial to consecutive windows of the signal to follow the shape of the randomly varying signal. In many cases, a drawback of this smoothing method is observed. If the frame length of the window is small, the denoised signal will remain noisy, and if the frame length of the window is large, the spectral resolution will be poor and causes distortion in spectral features.

Denoising using transforms (domain change) is an alternative to remove noise. Ethrentreich et al. compared denoising capability of the wavelet transform and Fourier transform and concluded that the wavelet transform performs better [16]. Also, Wentzell et al. used FIR filters, IIR filters, and Kalman filters as an alternative to denoise Raman spectra [17]. Greek et al. in 1995 and Craggs et al. used maximum entropy methods for signal recovery, but it requires solving a multivariate equation that is computationally expensive, and the problem of convergence was reported [18, 19].

Discrete wavelet transforms (DWT) decompose the signal into two components: approximations or the low-frequency sub-band and details or the high-frequency sub-bands. In Raman signal, random noise, fluorescence, and Raman peaks are high-frequency, low frequency, and mid-frequency components, respectively [14, 20]. These separate regimes of the noise, signal, and background make DWT a useful signal processing technique to denoise the Raman signal.

This paper focuses on the ability of the wavelet transform to remove cosmic ray spikes and denoise Raman signal. The double density dual-tree complex wavelet transforms (DD-DTCWT) are used to denoise, as well as to remove, spikes.

Theory. A spectral or Fourier transform representation of the signal is useful in many ways for process accuracy. However, in many cases, such representation is not sufficient because the time-evolution of the frequency components of the signal is not reflected in this transform [21, 22]. Alternatively, the wavelet transform of the signal produces better representation in the time and the frequency domain. It is a powerful signal processing tool that decomposes a signal or function into different frequency components, and then a resolution matched scale is used to study each component [23, 24]. DWT of the time series signal depends on the scale (or frequency) and the time, and thus the wavelet gives the time-frequency localization. Flow diagram for wavelet-based denoising of the noisy signal is as follows:

Noisy Signal $\rightarrow$ Wavelet Decomposition $\rightarrow$ Threshold determination $\rightarrow$ Denoisind $\rightarrow$ Reconstruct Signal.

Mathematically, the wavelet transform-based denoising can be denoted as

$$S = W^{-1}(Y(W(x))), \tag{3}$$

where W and W^{-1} denote forward and inverse wavelet transforms, respectively, and Y is the thresholding applied to the detail coefficients. DWT is an effective method of denoising, but a major drawback is the lack of translation invariance and directionality. which causes artifacts in the denoised signals.

The disadvantages of DWT are minimized using the CWT, but it is difficult to design complex filters that satisfy the perfect reconstruction restricting its use. Kingsbury [25] thus proposed DT-CWT, where the signal complex transform is calculated using two separates critically sampled discrete wavelet decompositions on the same signal working in parallel. For the perfect reconstruction of the signal, it is required that one tree have odd length filters, and another tree have even length filters. The two filters designed for the application of DT-CWT are real, and no complex arithmetic is involved. Two wavelet filters are designed in such a manner that they form a pair of Hilbert transforms, so that one tree gives real coefficients and the other gives imaginary coefficients. DT-CWT has improved properties like anti-aliasing effect, increased time-shift sensitivity, local phase information, and perfect reconstruction and has a redundancy of 2:1 for a 1-D signal independent of scales [26–28].

Double density discrete wavelet transform, on the other hand, is based on an over-sampled filter bank design. An overcomplete expansion dramatically enhances the shift-sensitivity of the transform, as shown by Selesnick [29]. Here, a single scaling function is used, and two distinct wavelets are designed to have an offset of one-half. The increased number of wavelets within the same scale provides a closer spacing between adjacent wavelets, thus approximating continuous wavelet transform. Wavelets obtained in DD-DWT are smoother than orthonormal wavelets with the same support. Oversampled DD-DWT has a redundancy of 2:1 independent of the level of decomposition. In undecimated DWT, redundancy grows with the level of decomposition [30].

DD-DWT and DT-CWT both have the same properties as overcomplete by a factor of 2, are nearly shift-invariant, and are based on a FIR perfect reconstruction. There are still significant differences in DD-DWT and DT-CWT such as:

1. Two wavelets in DT-CWT form the Hilbert transform pair, whereas two wavelets in DD-DWT are offset by one-half.

2. The degree of freedom to design filters in DD-DWT is greater compared to DT-CWT.

3. DT-CWT can be interpreted as a complex-valued wavelet transform, whereas DD-DWT cannot.

The benefits of DT-CWT and DD-DWT are combined in DD-DTCWT.

DD-DTCWT is overcomplete DWT, designed to have properties of DD-DWT and DT-CWT. It is based on two distinct scaling functions and four distinct wavelets.

$$Y_{h,i}(t), \qquad Y_{g,i}(t), \, i = 1, 2. \tag{4}$$

One pair of the wavelets is designed in such a way that they are half offset, so that the integer translation of one wavelet falls midway between the integer translation of other:

$$Y_{h,1}(t) = Y_{h,2}(t–0.5), \qquad Y_{g,1}(t) = Y_{g,2}(t–0.5). \tag{5}$$

Here, two wavelets $Y_{h,i}(t)$ are offset from one another by one-half, and so is $Y_{g,i}(t)$. Also, one pair of wavelets is designed in such a way that it is the Hilbert transform of ansother, so that two complex wavelets are obtained to implement the complex wavelet transform:

$$Y_{g,1}(t) = H\{Y_{h,1}(t)\}, \, Y_{g,2}(t) = H\{Y_{h,2}(t)\}. \tag{6}$$

The design for DD-DTCWT is based on a flat-delay filter, spectral factorization, and paraunitary filter bank completion, so that wavelets have vanishing moments and compact support. This leads to a smoother wavelet compared to dual-tree wavelets and forms the Hilbert transform pair, which is not available in double density wavelets. DD-DTCWT is four times more expensive. One tree of the filter bank gives the real part of the wavelet coefficients, whereas the other tree gives the imaginary part coefficients.

Method. The effectiveness of the denoising method using the wavelet transform depends on three parameters, namely the wavelet bases, decomposition level, and threshold method. The threshold method generally used in the wavelet transform is of two types: hard and soft thresholds. In the hard threshold method, the value of the detail coefficient smaller than the threshold value is set to zero, and when it is above the threshold value, it remains the same:

$$w_\lambda = \begin{cases} w, & |w| \geq \lambda, \\ 0, & |w| < \lambda. \end{cases} \tag{7}$$

On the other hand, in the soft threshold method, if the value of the detail coefficient is smaller than the threshold value, they are set to zero, but, if the value is above the threshold level, the absolute value of the threshold is subtracted from the wavelet coefficient:

$$w_\lambda = \begin{cases} \mathrm{sign}(w)(|w| - \lambda), & |w| \geq \lambda, \\ 0, & |w| < \lambda. \end{cases} \tag{8}$$

Popular threshold selection rules for the wavelet-based denoising includes the universal threshold, SURE threshold, the heuristic threshold, and the minimax threshold. At the start, Donoho proposed fixed value thresholding to denoise signals, calculated as

$$\lambda = \sqrt{2 \ln n / n}\,, \tag{9}$$

where n is the number of wavelet coefficients [31]. The noise dependent threshold is then obtained by modifying the fixed value threshold, known as the universal threshold. The universal threshold is calculated as

$$\lambda = \sigma \sqrt{2 \ln N}\,, \tag{10}$$

where N is the length of the noisy signal; σ is the standard deviation of noise estimated as

$$\sigma = \mathrm{median}(|Y_{ij}|)/0.6745, \tag{11}$$

where Y_{ij} are coefficient of the decomposition level. We use the universal threshold selection rule for threshold calculation.

The signal denoising procedure can be summarized as:

1. Noisy signal models: Signals under investigation are first imported in MATLAB, and Gaussian white noise of different SNR values are added to it.

2. Decomposition level: The level of decomposition is decided, and the forward DD-DTCWT is calculated.

3. Threshold calculation: The threshold value for each detail coefficient sub-band of the decomposed signal is estimated.

4. Threshold application: Apply the threshold value to the detail coefficient of both trees, real and imaginary coefficients.

5. Reconstruction: Inverse DD-DTCWT is applied to obtain the denoised signal.

6. Performance parameters: To evaluate the capability of the denoising method, performance parameters are calculated.

To verify the effectiveness of the proposed method, performance indicators are used. Signal to noise ratio (SNR) and root mean square error (RMSE) are used in this study. Mean square error is the average squared difference between the estimated value and the actual value. The square root of mean square error gives the RMSE, calculated as

$$\mathrm{RMSE} = \sqrt{\frac{\sum_{i=1}^{N}(x_i - \tilde{x}_i)^2}{N}}\,, \tag{12}$$

where x_i is the original signal, $\tilde{x}_i$ is the reconstructed signal, and N is the signal length. Another performance indicator considered here to evaluate the effectiveness of the method is SNR calculated in dB as the ratio of mean squared magnitude of the signal to the mean squared magnitude of the noise. SNR gives a qualitative analysis of the signal about the impact of noise on the signal, calculated as

$$\mathrm{SNR} = 10 \log(\delta^2/D), \tag{13}$$

where $\delta^2 = \frac{1}{N}\sum_{i=1}^{N}(x_i - \tilde{x})^2$, $D = \frac{1}{N}\sum_{i=1}^{N}(x_i - \tilde{x}_i)^2$, and $\tilde{x} = \frac{1}{N}\sum_{i=1}^{N}x_i$.

Result and discussion. For the spike removal study, actual Raman signal is used, and spikes of different intensity at different wavenumbers are simulated. For the denoising study, two types of data are used, namely, test benchmark signals (Bumps, Doppler, Blocks, and HeaviSine) and actual Raman signals. Raman

signals are obtained from the online Raman data bank. Noisy signal models are prepared for the test signals and Raman spectra under investigation by adding white Gaussian noise, considering noise as a linear combination to actual signal as described by Eq. (1). Gaussian noise added to signals have a standard deviation varying between 0 to 3 times of the lowest intensity of the signal. The processing of the signal is done using MATLAB 9.6.

Spike removal from Raman signal. At first, we tried to evaluate the capability of the wavelet transform to remove cosmic spikes by decomposing the signal to different levels, so that simultaneous denoising can be carried out. This is explored using the Raman spectrum of a forsterite-hydroxyapatite thin film on stainless steel. The Raman spectra exhibit an intense Raman band at 880 (*B*4) and 906 cm^{-1} (*B*5), with low intensity Raman peaks at 129 (*B*1), 300 (*B*2), 383 (*B*3), and 962 cm^{-1} (*B*6). The spectrum exhibits four simulated spikes at 366 (*S*1), 622 (*S*2), 746 (*S*3), and 1106 cm^{-1} (*S*4), with varying intensities from 1.6 times of the maximum intensity Raman band to 0.1 times of the maximum intensity Raman band, as shown in Fig. 1a. The simulated signal wavelet decomposition was performed using DD-DTCWT. Ideally, the spike removal requires that the approximation coefficient possesses properties such as a reduction in the Raman band intensity by the noise level, preservation of the Raman band profile, and removal of the spikes.
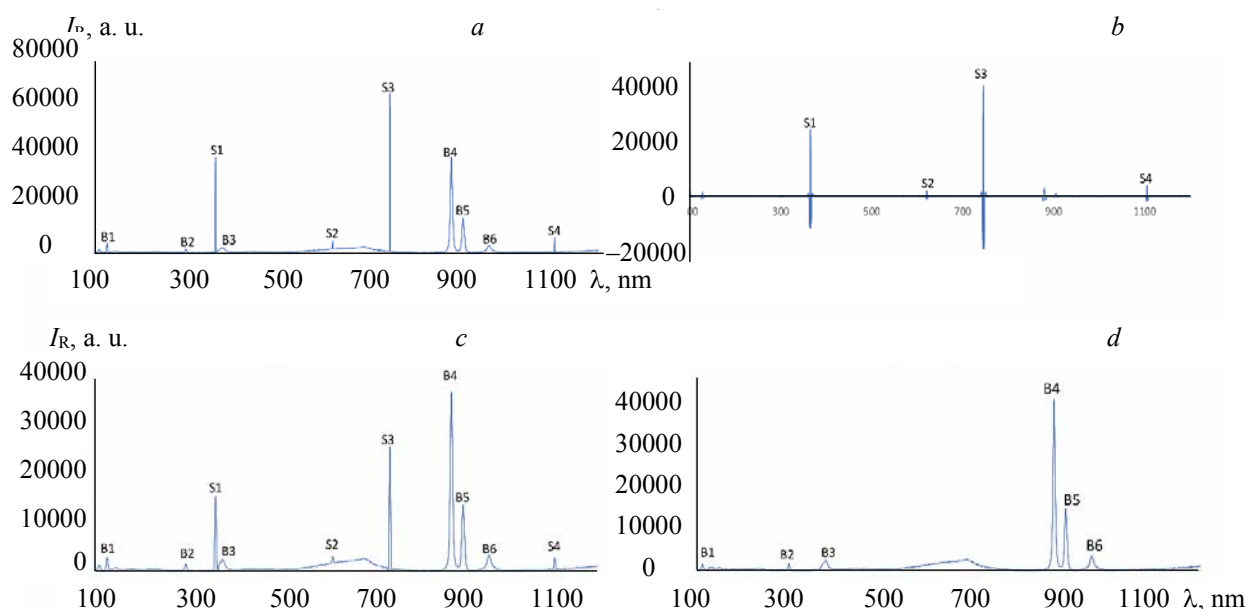
Fig. 1. a) Raman signal with simulated spikes; b) level 1 detail coefficient of DD-DTCWT; c) level 1 approximate coefficient of double density dual-tree complex wavelet transforms; d) despiked Raman signal.

From Figure 1c, it is evident that the desired properties not obtained as spikes also appear in the approximate coefficient along with Raman bands. It can be concluded from the above observation that simultaneous spike removal while denoising is not possible. Figure 1b shows a clear discrimination of spikes from Raman bands and noises that occur within the detail coefficients especially at first level details. If spike location from first-level detail coefficients can be projected into the appropriate location of the original Raman signal, spike removal can be performed. In Fourier analysis, this process is not possible, as time information is lost while time information is preserved in the wavelet transform. The additional argument of the peak width while locating the spike is applied in the time domain. It is observed that FWHM of the spike is generally near to 1 cm^{-1}, while for the Raman band it is much higher. This allows removing any location selected from the first-level decomposition that corresponds to Raman bands. After the appropriate location of the spike, an interpolation is applied to remove the spike. Figures 1a,d show the simulated spiked signal and signal after removing spikes.

Denoising of noisy Raman spectrum model. First, the denoising is applied to standard signals: Block, Bump, HeaviSine, and Doppler. Noisy signal models are obtained and denoised using DD-DTCWT, DT-CWT, DWT, and Savitzky–Golay smoothing (3rd and 1st order). Table 1 shows performance parameters for different signals.

TABLE 1. Signal to Noise Ratio and Root Mean Square Error for Test Signals

Denoising method	Block		Bump		HeaviSine		Doppler	
	SNR	RMSE	SNR	RMSE	SNR	RMSE	SNR	RMSE
Signal	15.06	0.1269	22.84	0.1777	24.54	0.1828	4.34	0.1778
DD-DTCWT	19.28	0.0755	28.21	0.0956	32.43	0.0736	12.61	0.0691
DT-CWT	18.36	0.0855	26.51	0.1165	30.56	0.0913	10.71	0.0884
DWT	14.45	0.1477	16.01	0.1119	29.66	0.1016	10.30	0.0930
SG3	15.40	0.1201	21.32	0.2116	28.91	0.1104	9.37	0.105
SG1	12.48	0.1606	19.61	0.2557	29.97	0.0977	11.1	0.083

N o t e. DD-DTCWT – Double density dual-tree complex wavelet transforms, DT-CWT – dual-tree complex wavelet transforms, DWT – discrete wavelet transforms, SG3 – Savitzky–Golay 3rd order smoothing, SG1 – Savitzky-Golay 1st order smoothing.

The above results show the superiority of DD-DTCWT in denoising the test signals, but the application of a denoising method to Raman signal is difficult due to the presence of low-intensity peaks. A denoising method is said to be effective if it is capable of increasing the signal to noise ratio (SNR) of the signal while retaining these small details. To study this, a pre-processed Raman signal of glucose, sucrose, and xanthan is obtained from an online available data bank, and noisy signal models are simulated by adding white Gaussian noise of different levels as obtained for previous signals. Figures 2a, b show the pre-processed Raman signal of xanthan and glucose. Figures 2c, d show the noisy Raman signal models with SNR for noisy signals as 25.59 and 17.55, respectively, and RMSE as 0.1814 and 0.1756, respectively. Denoising methods are applied, and the denoised signal parameters are calculated and tabulated in Table 2. Table 2 also shows SNR and RMSE data for the s ucrose Raman signal. Figures 2e,f show the Raman signal denoised by applying the proposed method. It can be observed that DD-DTCWT can denoise the noisy Raman signal effectively while retaining small features.
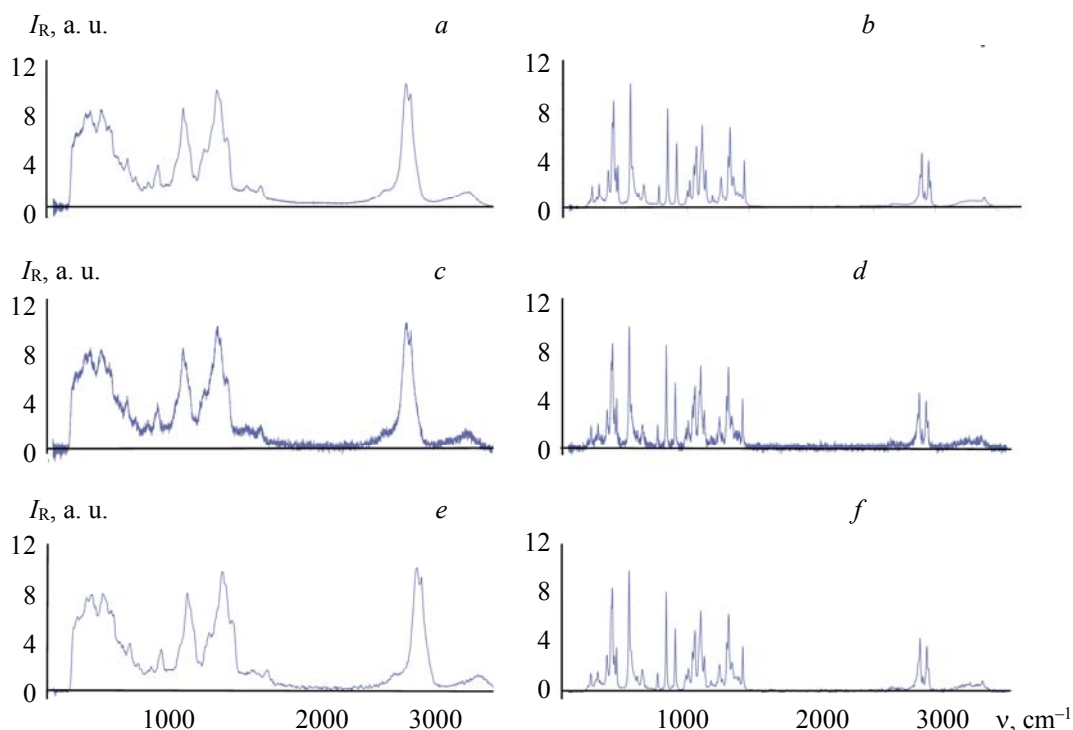
Fig. 2. a) Xanthan Raman Spectrum; b) glucose Raman Spectrum; c) xanthan Raman spectrum noise model; d) glucose Raman spectrum noise model; e) xanthan Raman spectrum denoised using the double density dual-tree complex wavelet transform; f) glucose Raman spectrum denoised using the double density dual-tree complex wavelet transform.

TABLE 2. Signal to Noise Ratio and Root Mean Square Error for Actual Raman Signals

Denoising method	Xanthan		Glucose		Sucrose	
	SNR	RMSE	SNR	RMSE	SNR	RMSE
Signal	25.5966	0.1814	17.5599	0.1756	18.7418	0.1794
DD-DTCWT	32.6063	0.0809	24.5431	0.0781	25.1465	0.0854
DT-CWT	30.8309	0.0993	23.3818	0.0899	24.5562	0.0920
DWT	30.3400	0.1051	22.3900	0.1007	23.5300	0.1035
SG3	29.3250	0.1182	21.9681	0.1059	23.2102	0.1075
SG1	30.5403	0.1027	23.0310	0.0927	23.6754	0.1011

N o t e. As in Table 1.

Figure 3 shows the variation of SNR and RMSE of the denoised signal using different methods as the noise level is varied. Here, it can be observed that for the high value of noise, both 1st order and 3rd order Savitzky–Golay works well, but as the noise level decreases, 1st order Savitzky–Golay smoothing capability to denoise signal continues decreasing as compared to 3rd order Savitzky–Golay smoothing. It can be concluded from these results that for denoising a Raman signal using Savitzky–Golay smoothing, it is required to perform random adjustments of the order and frame length of the smoothing method to obtain good results. Also, the DWT denoising capability is better than the Savitzky–Golay method, but SNR and RMSE are smaller than DD-DTCWT. DD-DTCWT always gives better SNR and RMSE and is not affected by the noise level introduced to the signal, from which it can be concluded that DD-DTCWT is a better method to denoise the Raman signal.
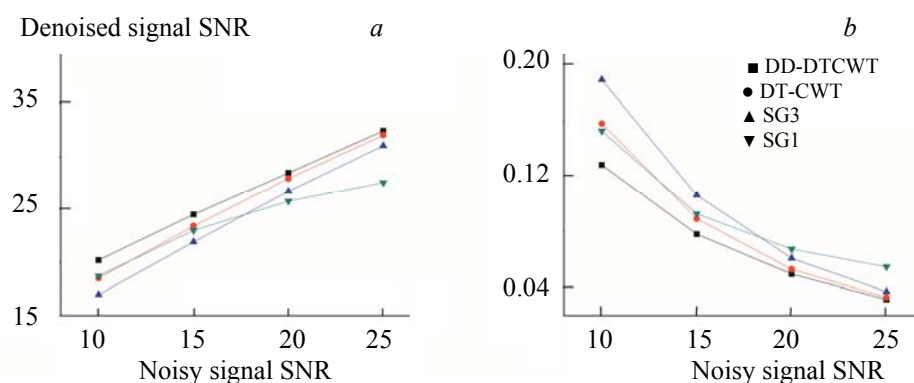
Fig. 3. Variation of the signal to noise ratio (a) and of the denoised the root mean square error signal (b) using different methods as the noise level is varie

Conclusions. Removal of spikes using the wavelet transform is not straightforward as obvious from the results, although spike removal and denoising can be carried out simultaneously by multiple decompositions of the signal. The first-level decomposition coefficient of the wavelet transform can discriminate spikes from noise and signal. The projection of spectral features from the wavelet transform domain to the original spectrum can be applied to remove spikes from the Raman spectrum. Sometimes the Raman peak may be included as a spike in projection to the time domain from the wavelet domain due to the first level wavelet coefficient value. Here, we used additional constraints as the peak width in the time domain to specifically select and remove the spike only from the spectrum. The results show that the proposed method works better with different intensity simulated spikes in the Raman signal.

Denoising the Raman spectrum is important for the quantitative and qualitative study of the spectrum. Savitzky–Golay smoothing is the most commonly used method for denoising the Raman signal, but the effectiveness of the method depends on the frame length of the window selected, SNR of the signal, and order of the filter used, as evident from the results. In this paper, we showed that the double-density dual-tree wavelet transform used for denoising of the signal gives better denoising results. The dual tree complex wavelet transform and discrete wavelet transform denoise the signal more efficiently, as compared to the standard Raman signal denoising method (Savitzky–Golay smoothing), and the addition of the double densi-

ty to the dual-tree complex wavelet transform adds features to the system that provide even better denoising results. The results showed that double density dual-tree complex wavelet transform has better denoising capability as compared to other commonly used methods. Denoising using DD-DTCWT is superior, independent of the noise level of the Raman signal.

Declaration of conflicting interest. The author(s) declared no potential conflicts of interest concerning the research, authorship, and/or publication of this article.

REFERENCES

1. C. V. Raman, K. S. Krishnan, *Nature*, **121**, 501 (1928).
2. C. N. Banwell, E. M. McCash, *Fundamentals of Molecular Spectroscopy*, **851**, McGraw-Hill, New York (1994).
3. H. Krishna, S. K. Majumder, P. Chaturvedi, M. Sidramesh, P. K. Gupta, *J. Biophotonics*, **7**, 690 (2014).
4. J. Filik, N. Stone, *Analyst*, **132**, 544 (2007).
5. J. M. Chalmers, M. Edwards, H. G. Hargreaves, *Infrared and Raman Spectroscopy in Forensic Science,* John Wiley & Sons, Ltd. (2012).
6. T. Bocklitz, A. Walter, K. Hartmann, P. Rösch, J. Popp, *Anal. Chim. Acta*, **704**, 47 (2011).
7. V. Deckert, W. Kiefer, *Appl. Spectrosc.*, **46**, 322 (1992).
8. G. Li, Second Int. Symp.Intell. Inform. Technology, *IEEE*, Shanghai, China, 535–539 (2008).
9. D. Groom, In: *Scientific Detectors for Astronomy*, Eds. P. Amico, J. W. Beletic, J. E. Beletic, Springer, Dordrecht, 81–94 (2004).
10. H. Choi, *Cosmic-Ray Interactions in Charged-Couple Devices in the DMTPC 4-Shooter Detector,* Doctoral dissertation, Massachusetts Institute of Technology (2013).
11. J. Zhao, *Appl. Spectrosc.*, **57**, 1368 (2003).
12. P. M. Ramos, I. Ruisánchez, *J. Raman Spectrosc.*, **36**, 848 (2005).
13. F. Ehrentreich, L. Sümmchen, *Anal. Chem.*, **73**, 4364 (2001).
14. H. Chen, W. Xu, N. Broderick, J. Han, *J. Raman Spectrosc.*, **49**, 1529 (2018).
15. A. Savitzky, M. J. E. Golay, *Anal. Chem.*, **36**, 1627 (1964).
16. F. Ehrentreich, *Anal. Bioanal. Chem.*, **372**, 115 (2002).
17. P. D. Wentzell, C. D. Brown, In: *Encyclopedia of Analytical Chemistry*, Ed. R. A. Meyers, John Wiley & Sons, Ltd., Chichester, UK, 5207 (2000).
18. L. S. Greek, H. G. Schulze, M. W. Blades, A. V. Bree, B. B. Gorzalka, R. F. B. Turner, *Appl. Spectrosc.*, **49**, 425 (1995).
19. C. Craggs, K. P. Galloway, D. J. Gardiner, *Appl. Spectrosc.*, **50**, 43 (1996).
20. R. Ramos, B. Valdez-Salas, R. Zlatev, M. Schorr Wiener, J. M. Bastidas Rull, *Int. J. Corros.*, 1 (**2017**).
21. L. A. Montejo, L. E. Suárez, Int. J. Adv. Struct. Eng., **5**, 26 (2013).
22. P. Karthikeyan, M. Murugappan, S. Yaacob, *Int. J. Electr. Eng. Inform.*, **4**, 306 (2012).
23. C. E. Heil, D. F. Walnut, *SIAM Rev.*, **31**, 628 (1989).
24. T. T. Cai, D. Zhang, D. Ben-Amotz, *Appl. Spectrosc.*, **55**, 1124 (2001).
25. N. Kingsbury, *Appl. Comput. Harmon. Anal.*, **10**, 234 (2001).
26. N. Kingsbury, *Philos. Trans. R. Soc. Lond. Ser. Math. Phys. Eng. Sci.*, **357**, 2543 (1999).
27. A. A. Petrosian, F. G. Meyer, *Wavelets in Signal and Image Analysis*, Kluwer Academic Publishers, Netherlands (2001).
28. I. W. Selesnick, *Appl. Comput. Harmon. Anal.*, **10**, 163 (2001).
29. I. W. Selesnick, *IEEE Trans. Signal Proc.*, **52**, 1304 (2004).
30. R. K. Sarawale, S. R. Chougule, *IEEE Second Int. Conf. Image Information Processing (ICIIP-2013)*, IEEE, Shimla, India, 219–224 (2013).
31. D. L. Donoho, I. M. Johnstone, G. Kerkyacharian, D. Picard, In: *Festschrift for Lucien Le Cam*, Springer, New York, 183–218 (1997).